Chinese Chemical Letters 34 (2023) 107995

Contents lists available at ScienceDirect

Chinese Chemical Letters

journal homepage: www.elsevier.com/locate/cclet

Two monofluoride-bridged Dy^{III} dimers with different magnetization dynamics

Mengmeng Wang[a,1], Xixi Meng[a,1], Ning Liu[a], Yi-Quan Zhang[b], Na Xu[a,*], Wei Shi[a,*], Peng Cheng[a,*]

[a] Department of Chemistry, Key Laboratory of Advanced Energy Materials Chemistry (MOE) and Renewable Energy Conversion and Storage Center (RECAST), College of Chemistry, Nankai University, Tianjin 300071, China
[b] Jiangsu Key Lab for NSLSCS, School of Physical Science and Technology, Nanjing Normal University, Nanjing 210023, China

ARTICLE INFO

Article history:
Received 6 October 2022
Revised 1 November 2022
Accepted 7 November 2022
Available online 10 November 2022

Keywords:
Fluoride ion bridge
Dinuclear Dy^{III} complexes
Magnetization dynamics
Single-molecule magnet
Suppressing QTM

ABSTRACT

As a monoatomic bridge, fluoride ion can transmit efficient magnetic interaction between lanthanide ions but its effect on tuning the magnetization dynamics has not been well understood. Herein, two monofluoride-bridged dinuclear dysprosium complexes $[Dy_2F(bbpen)_2(EtOH)_2]Br{\cdot}EtOH$ (**1**) and $[Dy_2F(bbppy)_2]Br{\cdot}2EtOH$ (**2**) with Dy-F-Dy angles of ~178° and their diamagnetic-ion diluted analogues **1′** and **2′** were synthesized. Magnetic studies reveal that **1** and **1′** barely show any magnetization dynamics, but **2** and **2′** exhibit strong magnetization dynamics. Systematical experimental analysis combined with *ab initio* calculations reveals that the different magnetization dynamics between **1** and **2** mainly originate from the effect of magnetic anisotropy by terminal ligand and bridging group of the chelating ligand, and the fluoride bridge can effectively suppress the quantum tunneling of the magnetization and turn on Orbach process in **2**.

The promise of a revolution in ultrasmall bistable nanodevices based on magnetic molecules relies upon understanding the structural factors governing the magnetization dynamics to achieve enhanced magnetic anisotropy [1–7]. As functional units, lanthanide (Ln^{III}) ions have the features of large ground state magnetic moment, strong spin-orbit coupling and ligand-field effect [8–10]. Tailoring the crystal field strength and coordination symmetry of Ln^{III} center has been efficiently applied to obtain magnetically anisotropic molecules [11–14]. The challenge to enhance the magnetic performance is from the complex relaxation pathways including quantum tunneling of magnetization (QTM), direct, Raman and Orbach processes, for which the key factors suppressing the fast magnetization dynamics that induce the loss of the magnetizations is still unclear [15–17].

Magnetic interactions between Ln^{III} ions influence the magnetization dynamic pathways [18–23]. Radicals have been demonstrated to transmit strong magnetic coupling and suppress QTM [19,24], but the synthesis of radical-based complexes is highly challenging and most of the products are not air-stable, hindering their practical applications. As alternatives, monoatomic bridges such as O^{2-}, OH^-, Cl^-, and O/SR^- (R = alkyl, aryl) have been studied as non-radical bridges with relatively convenient synthetic conditions [25–29]. However, fluoride ion, being the most electronegative species and hard Lewis base, has received limited attention in this field [30]. Recently, the first report of Dy^{III} complex bearing terminal fluoride ligand with strong and highly electrostatic Dy-F bond shows large axial crystal-field splitting and pronounced axial magnetic anisotropy [31]. However, the fluoride-bridged lanthanide complexes showing magnetization dynamics are still limited due to the unmanageable coordination ability of F^- ion [32–39].

Herein, we report two lone F^- ion bridged dinuclear Dy^{III} complexes $[Dy_2F(bbpen)_2(EtOH)_2]Br{\cdot}EtOH$ (**1**) and $[Dy_2F(bbppy)_2]Br{\cdot}2EtOH$ (**2**) produced by the reaction of $DyBr_3$ with H_2bbpen or H_2bbppy ligand containing different bridging groups in the presence of NH_4F (Scheme 1). The Dy-F-Dy angles are ~178° in both complexes. Antiferromagnetic interactions between Dy^{III} ions in **1** and **2** were observed. **1** barely shows any magnetization dynamics but **2** exhibits strong magnetization dynamics with effective energy barrier (U_{eff}) of 692 K and opened hysteresis loops. Magneto-structural correlation studies reveal that slight differences on the coordination sphere of Dy^{III} ions in **1** and **2** induced by terminal coordinated ethanol molecules and bridging groups of the ligands lead to very different magnetic anisotropy.

* Corresponding authors.
E-mail addresses: naxu@nankai.edu.cn (N. Xu), shiwei@nankai.edu.cn (W. Shi), pcheng@nankai.edu.cn (P. Cheng).
[1] These authors contributed equally to this work.

https://doi.org/10.1016/j.cclet.2022.107995
1001-8417/

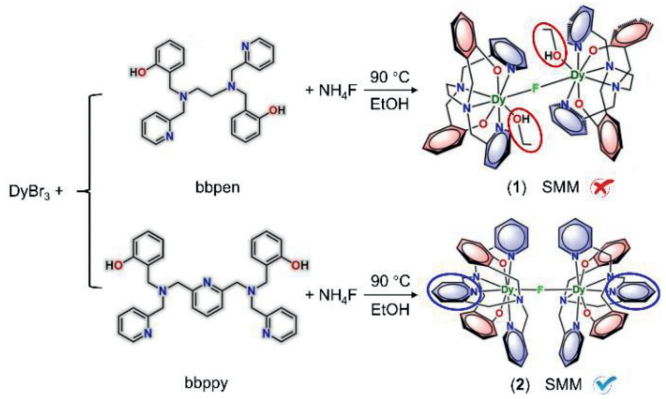

Scheme 1. Synthesis of **1** and **2**. The circles indicate main difference on the coordination structures.

Diamagnetic-ion dilution experiments demonstrate that F^- ion has valuable function in suppressing the quantum tunneling of the magnetization and turning on Orbach process in **2**.

1 and **2** crystallize in monoclinic *Cc* and *C2/c* space groups, respectively (Table S1 in Supporting information). Each unit cell contains two crystallographically independent Dy^{III} ions, which are bridged by one fluoride ion to form binuclear structures with the Dy-F-Dy bond angles of 177.9(5)° and 177.8(6)° and $Dy^{III}\cdots Dy^{III}$ distances of 4.4892(11) and 4.4515(11) Å for **1** and **2**, respectively (Fig. S1 in Supporting information). In **1**, both Dy^{III} ions are coordinated with two oxygen and four nitrogen atoms from one $bbpen^{2-}$ ligand, one fluoride ion and one ethanol molecule to form octa-coordinated spheres (Fig. 1). The Dy1-O_{bbpen} distances are 2.190(13) and 2.278(14) Å with the O_{bbpen}-Dy1-O_{bbpen} angle of 151.3(5)° (Table S2 in Supporting information). The Dy2-O_{bbpen} bond lengths are 2.204(12) and 2.290(12) Å with the O_{bbpen}-Dy2-O_{bbpen} angle of 152.4(5)°. The Dy1-F and Dy2-F bond lengths are 2.231(9) and 2.259(9) Å. The Dy-N distances range from 2.508(8) Å to 2.626(16) Å. In **2**, the Dy^{III} ions are surrounded by two oxygen and five nitrogen atoms from one H_2bbppy ligand and one fluoride ion to form octa-coordinated spheres. The Dy1-O_{bbppy} bond lengths are 2.192(5) and 2.225(6) Å with the O_{bbppy}-Dy1-O_{bbppy} angle of 149.5(4)°. The Dy2-O_{bbppy} bond lengths are 2.207(5) and 2.229(5) Å with the O_{bbppy}-Dy2-O_{bbppy} angle of 149.9(2)°. The bond lengths of Dy1-F and Dy2-F are both 2.226(4) Å. The Dy-N distances are 2.523(6)-2.681(6) Å. Although all Dy^{III} ions are eight-coordinated in both **1** and **2**, they feature different coordination spheres raised by the structural difference of the bridging groups of the ligands. The coordination symmetries are close to biaugmented trigonal prism (C_{2v}) for Dy^{III} ions in both **1** and **2** (Table S3 in Supporting information) [40,41]. The dinuclear units are further stacked to form supramolecular networks *via* C-H$\cdots\pi$ and hydrogen bonds interactions with the nearest intermolecular $Dy^{III}\cdots Dy^{III}$ distances of 10.172(3) and 9.904(9) Å for **1** and **2**, respectively (Figs. S2 and S3 in Supporting information). The high phase purities of them were confirmed by powder X-ray diffraction, elemental analyzes, thermogravimetric analyzes, and infrared spectra (Figs. S4 and S5 in Supporting information).

Direct current (dc) magnetic data at 1000 Oe dc field give the room-temperature $\chi_M T$ values of 27.49 and 27.45 cm^3 K/mol for **1** and **2**, respectively (Fig. 2), close to the expected value of 28.34 cm^3 K/mol for two uncoupled Dy^{III} ions. Upon cooling, $\chi_M T$ of **1** decreases gradually to a minimum of 24.78 cm^3 K/mol at 12 K, and then increases to 25.61 cm^3 K/mol at 2 K. For **2**, with temperature reducing, $\chi_M T$ declines slowly to 25.53 cm^3 K/mol at 16 K, followed by a sudden drop to a minimum of 21.36 cm^3 K/mol at 2 K. The decrease of $\chi_M T$ indicates thermal depopulation of the M_J states and/or antiferromagnetic interactions [42,43]. The rise of $\chi_M T$ for **1** at low temperature is related to the ferromagnetic dipolar interactions between Dy^{III} ions (see *ab initio* calculations below). The magnetizations are 10.23 and 12.75 Nβ at 70 kOe and 2 K for **1** and **2** (Fig. 2 inset), lower than the theoretical saturation value of 20 Nβ for two non-interacting Dy^{III} ions [44].

Alternating current (ac) magnetic data were measured at $H_{dc} = 0$ Oe to probe the magnetization dynamics. **1** exhibits very weak frequency-dependent out-of-phase (χ'') ac susceptibilities above 2 K (Fig. S6 in Supporting information). For **2**, in-phase (χ') and χ'' signals are frequency-dependent and peaks of χ'' signals were observed, indicating magnetization dynamics (Fig. 3a, Figs. S7 and S8 in Supporting information). The relaxation times (τ) were yielded from fitting ac susceptibilities by the generalized Debye model (Fig. 3b) [45]. The resulting α values in the range of 0.003–0.034 indicate narrow distribution of τ. The fitting slopes n of 4.5 and 10.3 from the τ *vs.* T^{-n} plot in log-log scale indicate that Raman process prevails in lower temperature range and Orbach process dominates in higher temperature range (Fig. 3c) [46]. Hence, the τ values were fitted using Eq. 1 (Fig. 3d) [47]:

$$\tau^{-1} = CT^m + \tau_0^{-1} exp(-U_{eff}/k_B T) \quad (1)$$

where C and m are empirical term for Raman relaxation, τ_0 is pre-exponential factor, and k_B is Boltzmann's constant. The best fitting resulted in $U_{eff}/k_B = 692$ K, $\tau_0 = 3.37 \times 10^{-11}$ s, $C = 4.45 \times 10^{-4}$ s^{-1} K^{-m}, and $m = 4.4$. The magnetic hysteresis loops of **2** show typical characterization of exchange-bias SMM [27,48] and keep opening to 5 K at a sweep rate of 20 Oe/s with coercive field of 118 Oe and remanent magnetization of 0.24 Nβ at 2 K (Fig. S9 in Supporting information). As field increases, the hysteresis loop opens first and then narrows at $H_{cross} \approx 998$ Oe (2 K, 20 Oe/s) because of the level crossing between low-lying exchange-based states [49]. Rhombus-shaped curves are observed when the sweep rate increases to 700 Oe/s.

To study the effect of magnetic interactions on magnetization dynamics and single-ion contributions, ac susceptibility measurements on the diamagnetic-ion diluted analogues **1′** and **2′** with the Dy^{III}:Y^{III} molar ratios of about 1:20 were performed. The χ' and χ'' data of **1′** are barely frequency dependent at $H_{dc} = 0$ Oe (Fig. S10 in Supporting information). The peak positions in plots of χ'' *vs.* T at different frequencies of **2′** emerge at the similar temperatures with those of **2** (Fig. S11 in Supporting information). However, the remarkable upturned tails below 10 K in χ'' *vs.* T plots for **2′** indicate prominent QTM. The χ'' *vs.* ν plots at different temperatures of **2′** show one set of peaks signal due to the similar coordination spheres of two crystallographic Dy^{III} ions (Fig. S12 in Supporting information). The τ values were acquired by fitting Cole-Cole plots (Fig. S13 in Supporting information). Linear fitting of the temperature-dependent τ in log-log scale gave slopes of 0.2 and 3.7, suggesting that QTM and Raman processes are prevailing in **2′** (Fig. S14 in Supporting information). Using Eq. 2 to fit the $\ln(\tau)$ *vs.* T^{-1} plot gave $C = 1.84 \times 10^{-3}$ s^{-1} K^{-m}, $m = 4.1$, and $\tau_{QTM} = 0.51$ s. Different from **2**, **2′** shows butterfly-shaped hysteresis loops up to 5 K with obvious zero-field magnetization loss (Fig. S15 in Supporting information). At 2 K and sweep rate of 20 Oe s^{-1}, the coercive field is 49 Oe and remanent magnetization is 0.25 Nβ.

$$\tau^{-1} = CT^m + \tau_{QTM}^{-1} \quad (2)$$

To further understand the experimental magnetization dynamics, complete-active-space self-consistent field (CASSCF) calculations on individual Dy^{III} fragments have been performed with MOLCAS 8.4 and SINGLE_ANISO programs [50,51]. The energy levels (cm^{-1}), g tensors and m_J components of the lowest eight Kramers doublets (KDs) are provided in Tables S4 and S5 (Support-

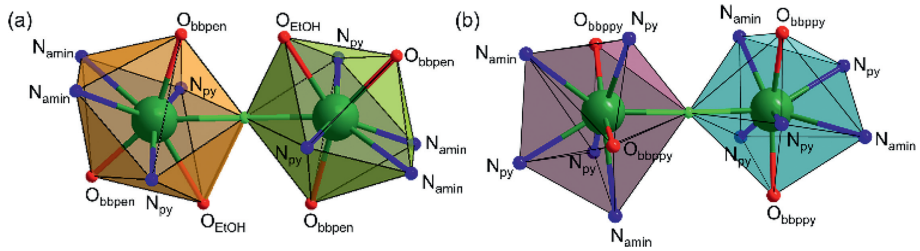

Fig. 1. The local coordination spheres of Dy^{III} ions in (a) **1** and (b) **2**.

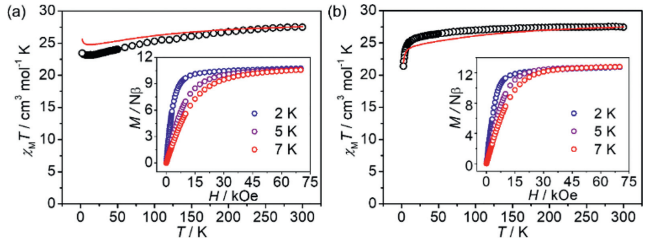

Fig. 2. Dc magnetic susceptibility data for (a) **1** and (b) **2**. The red lines represent fits to the data. Inset: *M vs. H* plots for (a) **1** and (b) **2**.

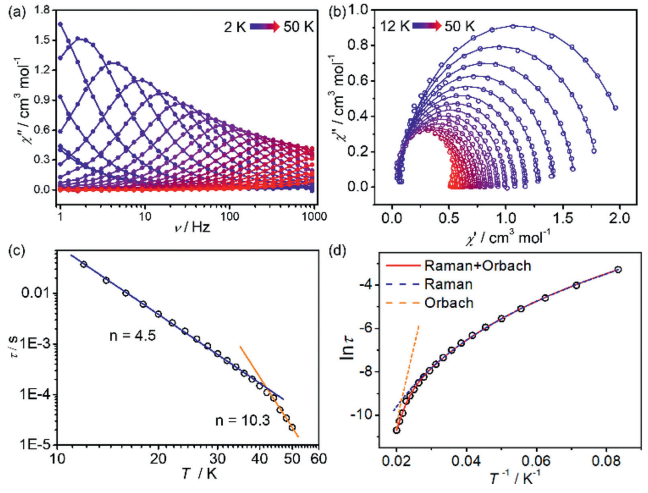

Fig. 3. (a) χ'' *vs.* ν plots at $H_{dc} = 0$ Oe and varying temperatures for **2**. (b) Cole-Cole plots for **2**. The solid lines are fitting results by the general Debye model. (c) Temperature-dependent relaxation times for **2** (log-log scale). The lines were fitted by $\tau = T^{-n}$ to give n values. (d) The ln(τ) *vs.* T^{-1} plots for **2**.

ing information). The *ab initio* calculated electronic states of the $^6H_{15/2}$ term of Dy^{III} ions are shown in Fig. 4, where the transversal magnetic moments in the ground KDs are all smaller than 10^{-2} μ_B. Hence QTM in the ground KDs could be suppressed. The transversal magnetic moments in the first excited KDs of Dy^{III} fragments for **1** are close to 10^{-1} μ_B, allowing quick QTM. The transversal magnetic moments in the first and second excited KDs of Dy^{III} fragments for **2** are ~10^{-2} and 10^{-1} μ_B, respectively. Hence, rapid QTM would happen in the second excited KDs. The calculated U_{eff} of individual Dy^{III} fragment in **1** and **2** are 283.6 cm^{-1} (408 K) (Dy1), 255.1 cm^{-1} (367 K) (Dy2), 532.2 cm^{-1} (766 K) (Dy1) and 524.7 cm^{-1} (755 K) (Dy2), respectively. We also calculated U_{eff} (Fig. S17 in Supporting information) according to the method put forward by Aravena recently (Supporting information) [52–54].

The calculated principal magnetic anisotropy axes (g_z) of the Dy^{III} sites lie along the shortest Dy-O_{phenol} direction (Fig. 5). The included angles between the magnetic axes on Dy^{III} ions are 172.6° and 124.0°. The angles between the magnetic axes and Dy-F bonds are 135.121° and 142.241° in **1**, and 92.860° and 90.632° in **2**. Other angles are shown in Tables S6 and S7 (Supporting information). The different angles between the magnetic axes and Dy-F bonds and the bond lengths of them are related with the relative position and strength of the shortest Dy-O_{phenol} and Dy-F bonds in the coordination spheres, which will influence the magnetic anisotropy of individual Dy^{III} ions and magnetic interaction between them. The calculated ground g_z are all ~20, suggesting that the exchange interactions between Dy^{III} ions can be approximately taken as Ising type (Fig. S18 in Supporting information). The dipolar magnetic couplings $\tilde{J}_{dip}$ were calculated as 1.28 cm^{-1} for **1** and −1.08 cm^{-1} for **2**, while exchange couplings $\tilde{J}_{exch}$ were fitted by comparing the computed and measured magnetic susceptibilities using POLY_ANISO program [55,56]. The fittings are shown in Fig. 2 with $\tilde{J}_{exch}$ of −1.98 and −0.70 cm^{-1} for **1** and **2**, respectively [57]. The stronger antiferromagnetic exchange interaction in **1** should relate to the larger included angle between the magnetic axes. The rise of $\chi_M T$ for **1** at low temperature could be from ferromagnetic dipolar interactions. Hence, the Dy^{III}···Dy^{III} interactions within lines model [58,59] are antiferromagnetic with $\tilde{J}_{total} = -0.70$ cm^{-1} for **1** and $\tilde{J}_{total} = -1.78$ cm^{-1} for **2** (Table S8 in Supporting information). The $\tilde{J}_{total}$ calculated from the crossing field H_{crosss} using the equation $H_{cross} = -\tilde{J}_{total}/2g_z\beta$ is 1.85 cm^{-1} for **2**, consistent with the POLY_ANISO results. The exchange energies and main values of the g_z for the lowest two exchange doublets are provided in Table S9 in Supporting information, where the g_z of the ground exchange states are 2.549 and 18.586 for **1** and **2**, respectively.

Magnetization dynamic analysis and *ab initio* calculations indicate that the magnetic anisotropy of **1** and **2** mainly originates from the individual Dy^{III} ions, and hence the very different magnetic behaviors between them should relate to different coordination environments of Dy^{III} ions. The lengths of axial Dy-O_{phenol} coordination bonds of **1** are longer than those of 2, indicating weaker axial crystal field of **1** than **2** (Fig. S1 and Table S2 in Supporting information). From *ab initio* calculations, the magnetic relaxation passes the first and second KDs of Dy^{III} ions in **1** and **2**, respectively. The calculated and experimental U_{eff} of **2** are close. The absence of experimental U_{eff} and frequency-dependent χ'' peaks for **1** from ac susceptibility measurement may be related to the coordination EtOH molecules that may induce adverse vibrational modes accelerating τ through barrier shortcuts [12,13].

By comparing the magnetization dynamics of **2** and **2´**, the role that bridging F^- ion plays can be revealed. First, the more pronounced upturned tails in χ'' *vs. T* plots at low temperatures (Figs. S7 and S11 in Supporting information) and more steep steps in hysteresis loops at around zero field (Figs. S9 and S15 in Supporting information) for **2´** than that of **2** indicate faster QTM at low temperatures for **2´** than that of **2**. Second, the peak positions in χ'' *vs.* ν plots at low temperatures for **2´** emerge at higher frequency than those for **2**, revealing smaller τ values or faster re-

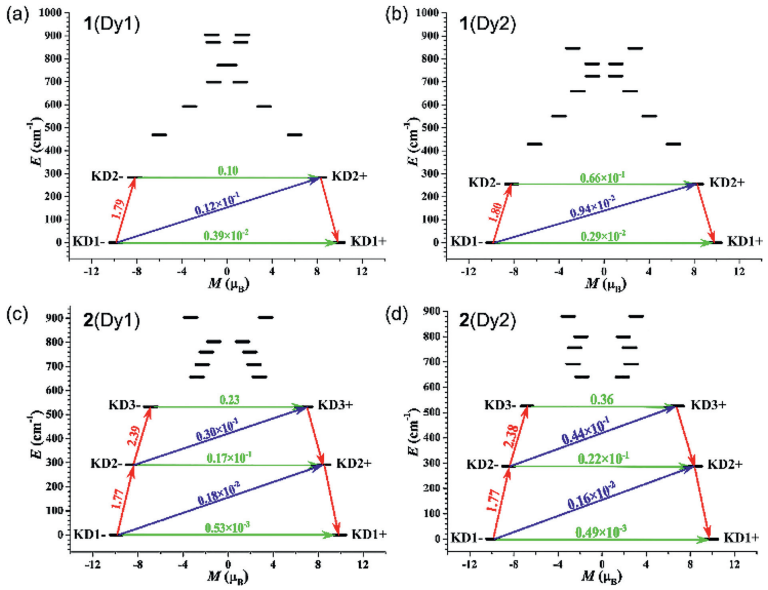

Fig. 4. The calculated electronic states of the $^6H_{15/2}$ term of (a) **1**(Dy1), (b) **1**(Dy2), (c) **2**(Dy1) and (d) **2**(Dy2).

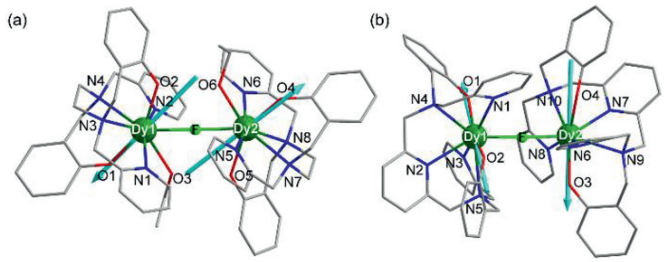

Fig. 5. Calculated orientations of local main magnetic axes on Dy^{III} ions in (a) **1** and (b) **2**.

laxation rate of **2**′ than that of **2** according to $\tau = 1/2\pi\nu$ (Fig. S16 in Supporting information). Furthermore, no effective energy barrier was obtained in the testing temperature and frequency range for 2́because the Orbach process may appear in higher temperature and frequency range.

In summary, two fluoride-bridged dinuclear Dy^{III} complexes with antiferromagnetic interactions between Dy^{III} ions were synthesized and display different magnetic behaviors. **1** is paramagnetic but **2** exhibits strong magnetization dynamics with U_{eff} of 692 K at $H_{dc} = 0$ Oe, the highest value reported to date for F^- ion bridged complexes. Structural analysis combining with theoretical analysis reveals that the replacement of terminal ethanol molecules by the pyridine groups in the coordination spheres of Dy^{III} ions leads to different magnetic anisotropies in **1** and **2**. Importantly, our result reveals that F^- ion as bridging ligand can form short coordination bond and transmit magnetic interaction between Dy^{III} ions which can efficiently suppress QTM at low temperatures and facilitate the observation of Orbach process in **2**. This work highlights the importance of using fluoride ion as bridge to suppress fast magnetization dynamics and may provide a new way for the development of multinuclear lanthanide complexes with tailored magnetic performance.

Declaration of competing interest

The authors declare that they have no known competing financial interests or personal relationships that could have appeared to influence the work reported in this paper

Acknowledgments

This work is supported by the National Key R&D Program of China (No. 2018YFA0306002), the National Natural Science Foundation of China (Nos. 21971123 and 21973046), the Natural Science Foundation of Tianjin (No. 18JCJQJC47200).

Supplementary materials

Supplementary material associated with this article can be found, in the online version, at doi:10.1016/j.cclet.2022.107995.

References

[1] R. Sessoli, D. Gatteschi, A. Caneschi, et al., Nature 365 (1993) 141–143.
[2] D. Gatteschi, R. Sessoli, J. Villain, Molecular Nanomagnets, Oxford University Press, Oxford, 2006.
[3] A. Zabala-Lekuona, J.M. Seco, E. Colacio, Coord. Chem. Rev. 441 (2021) 213984.
[4] Y. Ma, Y.Q. Zhai, Q.C. Luo, et al., Angew. Chem. Int. Ed. 61 (2022) e202206022.
[5] M. Wang, Y. Guo, Z. Han, et al., Inorg. Chem. 61 (2022) 9785–9791.
[6] X. Zhang, V. Vieru, X. Feng, et al., Angew. Chem. Int. Ed. 54 (2015) 9861–9865.
[7] M. Wang, X. Meng, F. Song, et al., Chem. Commun. 54 (2018) 10183–10186.
[8] J.D. Rinehart, J.R. Long, Chem. Sci. 2 (2011) 2078–2085.
[9] Z.H. Zhu, M. Guo, X.L. Li, et al., Coord. Chem. Rev. 378 (2019) 350–364.
[10] K. Jia, X. Meng, M. Wang, et al., Chem. Commun. 57 (2021) 3607–3610.
[11] J.L. Liu, Y.C. Chen, M.L. Tong, Chem. Soc. Rev. 47 (2018) 2431–2453.
[12] C.A.P. Goodwin, F. Ortu, D. Reta, et al., Nature 548 (2017) 439–442.
[13] F.S. Guo, B.M. Day, Y.C. Chen, et al., Science 362 (2018) 1400–1403.
[14] K. Liu, X. Zhang, X. Meng, et al., Chem. Soc. Rev. 45 (2016) 2423–2439.
[15] D. Gatteschi, R. Sessoli, Angew. Chem. Int. Ed. 42 (2003) 268–297.
[16] M.J. Giansiracusa, A.K. Kostopoulos, D. Collison, et al., Chem. Commun. 55 (2019) 7025–7028.
[17] Y.S. Ding, T. Han, Y.Q. Zhai, et al., Chem. Eur. J. 26 (2020) 5893–5902.
[18] C.A. Gould, R.A. McClain, D. Reta, et al., Science 375 (2022) 198–202.
[19] S. Demir, M.I. Gonzalez, L.E. Darago, et al., Nat. Commun. 8 (2017) 2144.
[20] X. Zhang, S. Liu, V. Vieru, et al., Chem. Eur. J. 24 (2018) 6079–6086.
[21] Y.C. Chen, M.L. Tong, Chem. Sci. 13 (2022) 8716–8726.
[22] K. Liu, W. Shi, P. Cheng, Coord. Chem. Rev. 289 (2015) 74–122.
[23] H. Li, X. Meng, M. Wang, et al., Chin. J. Chem. 37 (2019) 373–377.
[24] S. Demir, I.R. Jeon, J.R. Long, et al., Coord. Chem. Rev. 289 (2015) 149–176.
[25] J. Xiong, H.Y. Ding, Y.S. Meng, et al., Chem. Sci. 8 (2017) 1288–1294.
[26] F. Tuna, C.A. Smith, M. Bodensteiner, et al., Angew. Chem. Int. Ed. 124 (2012) 7082–7086.
[27] Y.S. Meng, J. Xiong, M.W. Yang, et al., Angew. Chem. Int. Ed. 59 (2020) 13037–13043.
[28] Y.N. Guo, G.F. Xu, W. Wernsdorfer, et al., J. Am. Chem. Soc. 133 (2011) 11948–11951.
[29] T. Han, M.J. Giansiracusa, Z. Li, et al., Chem. Eur. J. 26 (2020) 6773–6777.
[30] K.S. Pedersen, M.A. Sørensen, J. Bendix, Coord. Chem. Rev. 299 (2015) 1–21.
[31] L. Norel, L.E. Darago, B. Le Guennic, et al., Angew. Chem. Int. Ed. 57 (2018) 1933–1938.

[32] Q. Zhou, F. Yang, D. Liu, et al., Inorg. Chem. 51 (2012) 7529–7536.
[33] G. Brunet, F. Habib, I. Korobkov, et al., Inorg. Chem. 54 (2015) 6195–6202.
[34] Q. Yuan, Y.S. Meng, Y.Q. Zhang, et al., Inorg. Chem. Front. 9 (2022) 2336–2342.
[35] Y. Huo, Y.C. Chen, S.G. Wu, et al., Inorg. Chem. 58 (2019) 1301–1308.
[36] J. Corredoira-Vázquez, C. González-Barreira, M. Fondo, et al., Inorg. Chem. 61 (2022) 9946–9959.
[37] B.K. Ling, Y.Q. Zhai, P.B. Jin, et al., Matter (2022), doi:10.1016/j.matt.2022.07.009.
[38] S.K. Langley, C.M. Forsyth, B. Moubaraki, et al., Dalton Trans. 44 (2015) 912–915.
[39] K.R. Vignesh, S.K. Langley, K.S. Murray, et al., Chem. Eur. J. 23 (2017) 1654 -166.
[40] M. Pinsky, D. Avnir, Inorg. Chem. 37 (1998) 5575–5582.
[41] M. Llunell, D. Casanova, J. Cirera, et al., SHAPE Program, Version 2.0, Universitat de Barcelona, Barcelona, Spain, 2010.
[42] Y.X. Wang, Y. Ma, Y. Chai, et al., J. Am. Chem. Soc. 140 (2018) 7795–7798.
[43] X.L. Li, L. Zhao, J. Wu, et al., Chem. Sci. 13 (2022) 10048–10056.
[44] T.P. Latendresse, N.S. Bhuvanesh, M. Nippe, J. Am. Chem. Soc. 139 (2017) 8058–8061.
[45] K.S. Cole, R.H. Cole, J. Chem. Phys. 9 (1941) 341–351.
[46] A. Abragam, B. Bleaney, Electron Paramagnetic Resonance of Transition Ions, Oxford University Press, 1970.
[47] K.R. Meihaus, S.G. Minasian, W.W. Lukens, et al., J. Am. Chem. Soc. 136 (2014) 6056–6068.
[48] J. Long, F. Habib, P.H. Lin, et al., J. Am. Chem. Soc. 133 (2011) 5319–5328.
[49] X. Yi, K. Bernot, F. Pointillart, et al., Chem. Eur. J. 18 (2012) 11379–11387.
[50] F. Aquilante, J. Autschbach, R.K. Carlson, et al., J. Comput. Chem. 37 (2016) 506–541.
[51] L.F. Chibotaru, L. Ungur, A. Soncini, Angew. Chem. Int. Ed. 47 (2008) 4126–4129.
[52] D. Aravena, J. Phys. Chem. Lett. 9 (2018) 5327–5333.
[53] B. Yin , C.C. Li, Phys. Chem. Chem. Phys. 22 (2020) 9923–9933.
[54] A. Castro-Alvarez, Y. Gil, L. Llanosa, et al., Inorg. Chem. Front. 7 (2020) 2478–2486.
[55] L.F. Chibotaru, L. Ungur, C. Aronica, et al., J. Am. Chem. Soc. 130 (2008) 12445–12455.
[56] L. Ungur, W. van den Heuvel, L.F. Chibotaru, New J. Chem. 33 (2009) 1224–1230.
[57] S.K. Langley, D.P. Wielechowski, V. Vieru, et al., Angew. Chem. Int. Ed. 52 (2013) 12014–12019.
[58] M.E. Lines, J. Chem. Phys. 55 (1971) 2977–2984.
[59] K.C. Mondal, A. Sundt, Y.H. Lan, et al., Angew. Chem. Int. Ed. 51 (2012) 7550–7554.